Supporting Information: Small gold nanoparticles synthesized with sodium citrate and heavy water: Insights into the reaction mechanism

Isaac Ojea-Jiménez[a§*], *Francisco M. Romero*[b], *Neus G. Bastús*[c‡], *Victor Puntes*[c,d]*

[a]Endor Nanotechnologies, S.L.; [b]Institut de Ciència Molecular; [c]CIN2 (Institut Català de Nanotecnologia-CSIC); [d]Institut Català de Recerca i Estudis Avançats (ICREA); [§]Current Address: Institut Català de Nanotecnologia; [‡]Current Address: Institut für Physikalische Chemie, Universität Hamburg

S1: TEM characterization and size distribution of Au NPs after a single centrifugation step.

The Au NP size distribution obtained in the presence of D_2O was easily narrowed upon centrifugation. Thus, after a single centrifugation step of 15 minutes at 40.000 rcf the SPR peak shifts from 512.5 nm to 511.5 nm in the UV-Vis spectrum and the size distribution decreases from 5.5 ± 1.1 nm to 4.4 ± 0.7 nm.

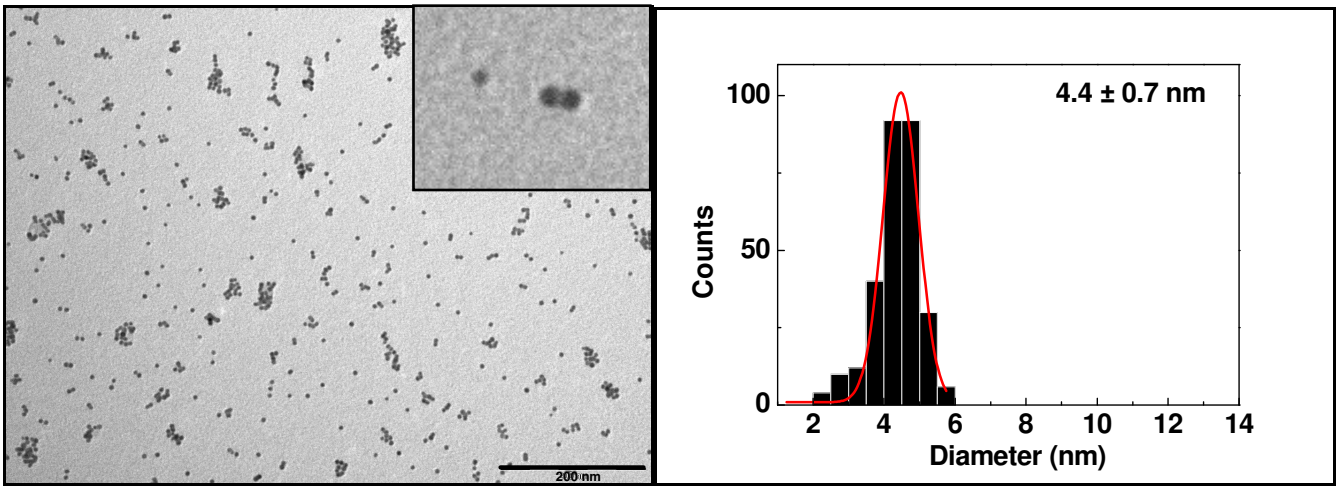

S2: DLS and Z-Potential measurements corresponding to Au NPs synthesized at 100 ºC in D_2O (5 nm) and H_2O (9 nm).

Sample	Hydrodynamic Diameter nm (PdI)
AuNP (5 nm)	9.7 (0.19)
AuNP (9 nm)	15.4 (0.39)
Sample	**Z-potential mV (std. Dev. In mV)**
AuNP (5 nm)	-33.9 (8.8)
AuNP (9 nm)	-43.0 (13.9)

S3: Mass spectrometry analysis of the sodium citrate species present in solution at 100 ºC in D_2O.

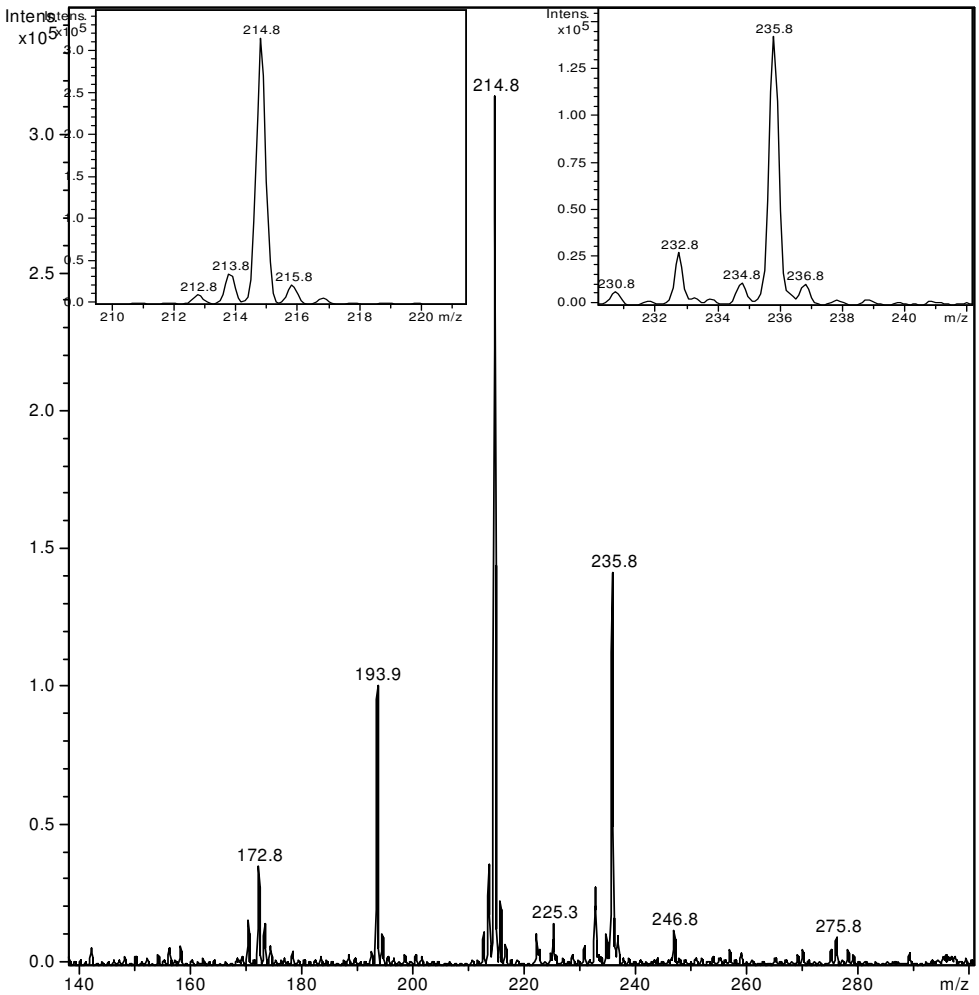

S4: Time evolution of the UV-Vis absorbance spectra of Au NPs synthesized both in H_2O and D_2O at 90 ºC.

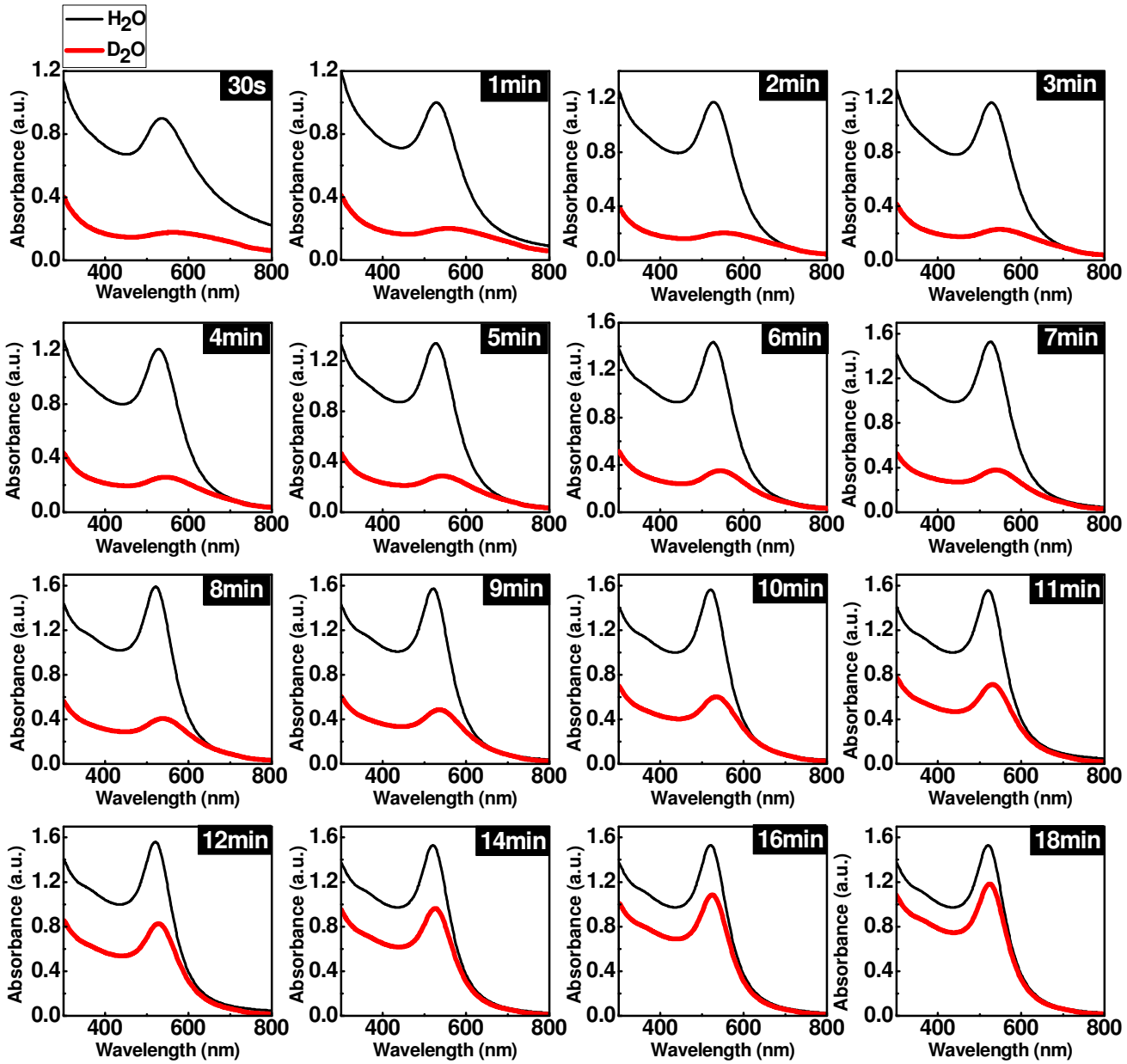

S5: Time evolution of the colors of Au NPs solutions synthesized at 90 ºC in H_2O and D_2O.

H_2O

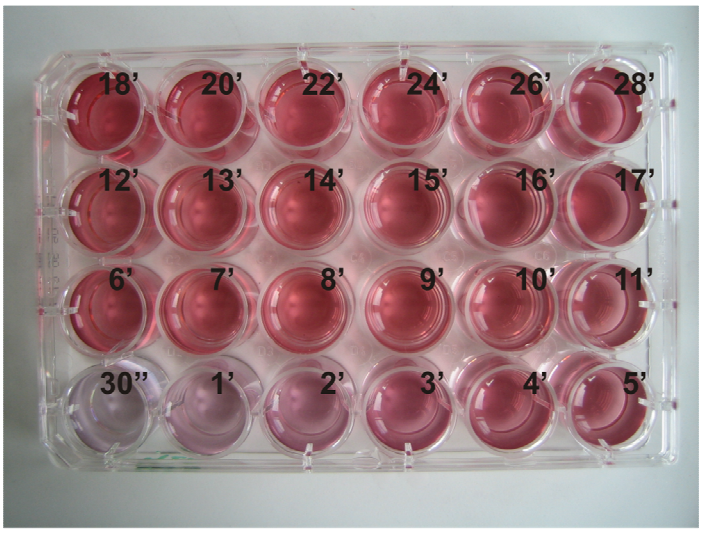

D_2O

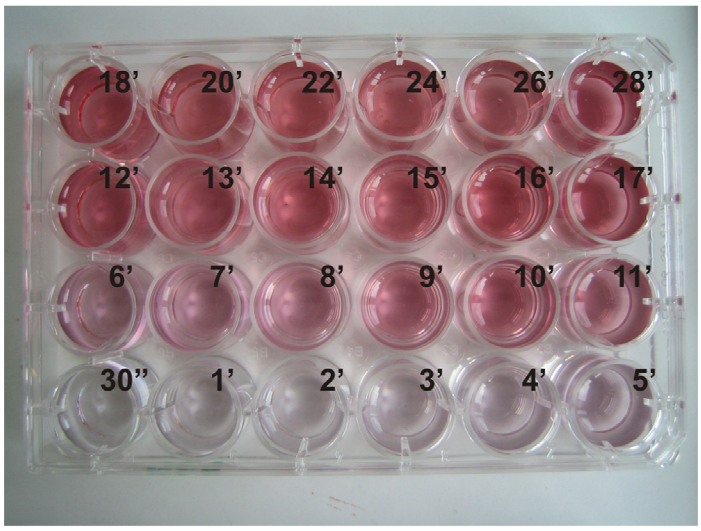

S6: FT-IR analysis corresponding to a) Au NP immediately after their formation at 100 ºC in H_2O, b) Au NP precipitated and dried, c) sodium citrate and d) 1,3-dicarboxyacetone.

FT-IR measurement of an aqueous solution of Au NPs was difficult due to the presence of the large amount of solvent, which gave strong signals at 3342 and 1636 cm^{-1} corresponding to the stretching and bending vibrational modes of H_2O, respectively. In spite of that, when a liquid aliquot of the sample was taken during the process of formation of Au NPs (a) (5 minutes after injection of $HAuCl_4 \cdot 3H_2O$), it could be observed (though the poor intensity) some peaks which could not be perfectly correlated neither with 1,3-dicarboxyacetone (b) nor with sodium citrate (c). This could be explained by the presence of a mixture of these compounds, which could also include other

decomposition/decarboxilation products such as acetoacetate or acetone resulting in a complex spectrum. However, it could clearly be observed a peak at 1699 cm^{-1}, which is in the region characteristic for ketone compounds and that can be attributed to decarboxylated products of sodium citrate. Furthermore, the band corresponding to the stretching of CO_2 at 2369 cm^{-1} was much more intense in the aqueous sample of Au NPs than in the reference materials (i.e. citrate or 1,3-dicarboxyacetone), which make one suspicious about its contribution being only from atmospheric gases or if it mostly comes from the release of CO_2 from the decarboxylation reaction. We must note that spectrum (a) was measured before (b) and (c), which rules out the possible increase of CO_2 in the atmosphere due to the breathing of the analyst. We also note that FT-IR spectra were measured by duplicate.

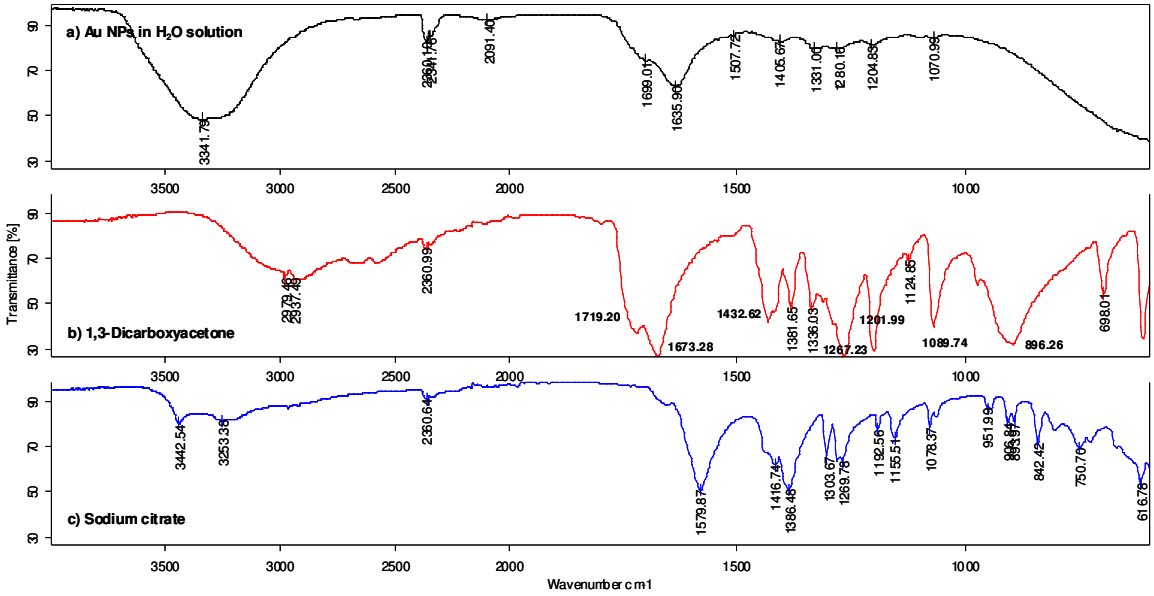

When the Au NP sample was precipitated (by addition of NaCl and centrigugation) and dried before the FT-IR measurement, the resulting spectrum (d) could be well correlated with the spectrum of sodium citrate (c). These results agree with what would be expected for a dry sample of Au NPs, since in the solid residue only the citrate molecules attached to the surface of the NPs are left while other more volatile and unstable ketone compounds are removed during the drying process.

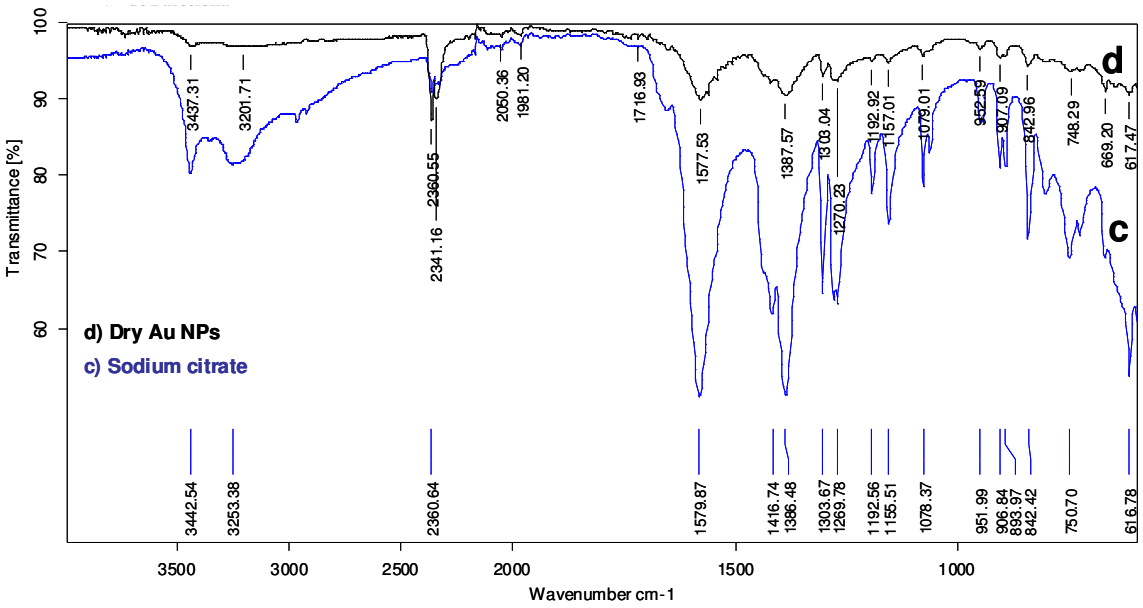
d) Dry Au NPs
c) Sodium citrate
Transmittance [%]
Wavenumber cm-1
d
c
3437.31
3201.71
2360.55
2341.16
2050.36
1981.20
1716.93
1577.53
1387.57
1303.04
1270.23
1192.92
1157.01
1079.01
952.59
907.09
842.96
748.29
669.20
617.47
3442.54
3253.38
2360.64
1579.87
1416.74
1386.48
1303.67
1269.78
1192.56
1155.51
1078.37
951.99
906.84
893.97
842.42
750.70
616.78